

BUPTCMCC-6G-CMG+: A GBSM-Based ISAC Standard Channel Model Generator

Changsheng ZHAO¹, Jianhua ZHANG^{1*}, Yuxiang ZHANG^{1*}, Lei TIAN¹, Heng WANG¹, Hanyuan JIANG¹, Yameng LIU¹, Wenjun CHEN¹, Tao JIANG² & Guangyi LIU²

¹State Key Laboratory of Networking and Switching Technology, Beijing University of Posts and Telecommunications, Beijing 100876, China;

²Future Research Laboratory, China Mobile Research Institute, Beijing 10053, China

Abstract Integrated sensing and communication (ISAC) has been recognized as the key technology in the vision of the sixth generation (6G) era. With the emergence of new concepts in mobile communications, the channel model is the prerequisite for system design and performance evaluation. Currently, 3GPP Release 19 is advancing the standardization of ISAC channel models. Nevertheless, a unified modeling framework has yet to be established. This paper provides a simulation diagram of ISAC channel modeling extended based on the Geometry-Based Stochastic Model (GBSM), which is compatible with existing 5G channel models and the latest progress in 3GPP standardization. We first introduce the progress of the ISAC channel model standard in general. Then a concatenation channel modeling approach considering team standardization proposals is presented which is implemented on the BUPTCMCC-6G-CMG+ channel model generator. We validated the model in cumulative probability density function (CDF) in statistical extension of angle and delay, and radar cross section (RCS). Simulation results show that the proposed model can realistically characterize the feature of concatenation and RCS within the ISAC channel. At the same time, the proposed method maintains an efficient simulation.

Keywords Channel model generator, concatenation, ISAC channel, RCS, 3GPP standardization.

1 Introduction

6G mobile communication technology is anticipated to enhance 5G communication capabilities roundly, including high capacity, low latency, and high reliability, while achieving native intelligence, ISAC, and ubiquitous connectivity [1]. The boundary between the physical and digital realms is expected to become increasingly indistinct, offering users a ubiquitous and immersive experience [2]. Concerns of communication systems will need to expand from information transmission to information acquisition and information processing [3]. ISAC is the essential technology necessary to achieve the information paradigm transformation described above. ISAC technology can facilitate the implementation of diverse use cases, particularly in localization, tracking, imaging, and the detection of target type, speed, and direction. These capabilities will enable applications in autonomous driving, industrial automation, digital twin reconstruction of physical environments, gesture detection, and activity recognition [4–8]. The sensing information obtained from ISAC can facilitate the development of smart homes, factories, smart cities, and intelligent transportation systems. Meanwhile, ISAC technology introduces new performance metrics relative to traditional communication technologies, including detection probability, sensing capacity density, sensing accuracy, and resolution for speed, angle, and delay [9].

The transmission medium between the transmitter and receiver establishes the performance limits of communication systems. The wireless channel plays a vital role in researching and evaluating wireless communication technologies. [10–12]. The performance evaluation of the ISAC system introduces new requirements for channel models, particularly regarding sensing modes and scenarios, sensing use cases, and channel modeling methodologies. Considering sensing modes, current channel models usually utilize

* Corresponding author (email: jhzhang@bupt.edu.cn, zhangyx@bupt.edu.cn)

Bi-static modes for communication. Sensing applications necessitate considering the case of Mono-static channel models for self-sensing. Thus, ISAC channel models should incorporate both Mono-static and Bi-static sensing modes. Secondly, concerning sensing use cases involving sensing targets, ISAC applications expand the evaluation criteria to include target detection, localization, identification, and tracking. Examples encompass intrusion detection, unmanned aerial vehicle (UAV) tracking, vehicle-to-everything (V2X) communications, and the identification of diverse target types and sizes. That requires using the scattering properties of RCS, polarization characteristics, delay, and Doppler information of electromagnetic waves as they interact with targets. Consequently, channel models should integrate the RCS characteristics of various targets. Moreover, with respect to modeling methodologies, it is imperative to account for the cascaded characteristics of channels interacting with targets while coupling with existing standard communication channel models [13–16].

So far, the standardization of ISAC channel models by 3GPP has held five conferences from #116 to #118-bis, wherein ISAC scenarios, types of sensing targets, sensing modes, and general channel model frameworks have been defined. The defined scenarios encompass traditional urban micro (UMi), urban macro (UMa), rural macro (RMa), and indoor hotspot (InH) scenarios, in addition to V2X, UAV, and industrial Internet of things (IIoT) scenarios. Accordingly, sensing targets are classified into five categories: humans, vehicles, UAVs, automated guided vehicles (AGVs), and obstacles as shown in Table 1. Sensing modes are categorized into Bi-static and Mono-static, which are further subdivided into six specific use cases based on whether the sensing device is a user terminal (UT) or a base station (BS): BS-UT-Bi, BS-BS-Bi, UT-UT-Bi, UT-BS-Bi, UT-UT-Mono, and BS-BS-Mono [17]. In the framework of channel modeling, the ISAC channel is defined as the combination of the target channel and the background channel. The target channel includes all channel components that interact with targets, whereas the background channel comprises all other elements that do not engage with targets.

For ISAC channel simulation, a channel model that separately generates communication and sensing clusters based on the 3GPP model, and utilizes sensing echoes for perception, has been proposed [18]. Some studies introduce the concept of shared clusters to explain the phenomenon of scattering body reuse between the communication and sensing channels [5, 19, 20]. Some studies focus on deterministic ISAC channel modeling [21, 22]. However, these studies do not align with the target and background channel modeling framework or the cascading channel method in 3GPP Rel-19. Most of these approaches use single-station echoes for perception and do not support Bi-static sensing modes.

To the authors' knowledge, no unified ISAC channel simulation framework compatible with the latest 3GPP standardization progress has been proposed. Considering that standardization is primarily followed by industry and the existing standardization framework has not been fully finalized, we present our solution based on our team's work in ISAC standardization and our understanding of standardized channel simulation. We hope this will contribute to advancing both the academic field and the establishment of standardized models. The contributions and innovations of this paper are outlined as follows:

(a) Different from existing ISAC channel simulation models [18–22], we propose a unified ISAC channel simulation framework based on the 3GPP Rel-19 ISAC channel fundamental structure, where the ISAC channel is the combination of the target and background channels. This framework maximizes the use and compatibility with existing 5G standardized channel models. It incorporates our team's contributions to the standardization process, offering a solution that aligns with the latest standardized progress and consensus in ISAC channel modeling.

(b) The effective ISAC channel simulation method has been validated.

- We compared and analyzed the down-section simulation results for the 8 cascading options presented in the RAN1 #118-bis meeting, explaining the mechanisms behind the results. Based on it, we propose a simulation method for ISAC cascading channels.

- A unified RCS simulation model is introduced, which considers the progress of the 116-118bis meetings and incorporates our team's RCS measurement results. This model applies to various target types, accounting for factors such as large-scale, small-scale, statistical, and deterministic elements.

- We propose a solution for combining the target and background channels, compatible with two existing standardized approaches: one where the target channel is included in the background channel and the other where the target channel is directly added to the background channel.

- Key performance evaluation metrics for ISAC are provided, along with a brief analysis of the underlying mechanisms for each metric.

The paper is organized as follows. Section 2 describes the simulation architecture in detail. Section

Table 1 3GPP ISAC Standardization Focused Scenarios

Sensing targets	Scenarios
UAVs	RMa-AV, UMa-AV, UMi-AV
Humans indoors	InF, InH, UMi, UMa, RMa
Automotive vehicles	Highway, Urban grid, UMi, UMa, RMa
Automated guided vehicles	InF
Objects creating hazards on road/railways	Highway, Urban grid, Urban grid HST

3 reports on evaluation metrics for ISAC. Then, Section 4 presents the simulation results from both concatenation and RCS. Section 5 concludes the paper.

2 Simulation Architecture

Building upon the current advancements in 3GPP standardization efforts and the GBSM simulation framework, this paper proposes an ISAC channel simulation framework designed for future standardization, which is integrated into the BUPTCMCC-6G-CMG+ channel model generator. The key characteristics of ISAC channels—including cascaded features, RCS polarization, scattering properties, and the coupling between target and background channels are considered to establish a unified model for ISAC channel simulation. In this model, the ISAC channel is divided into two components: the target channel and the background channel. The geometric schematic of the model is shown in Figure 1.

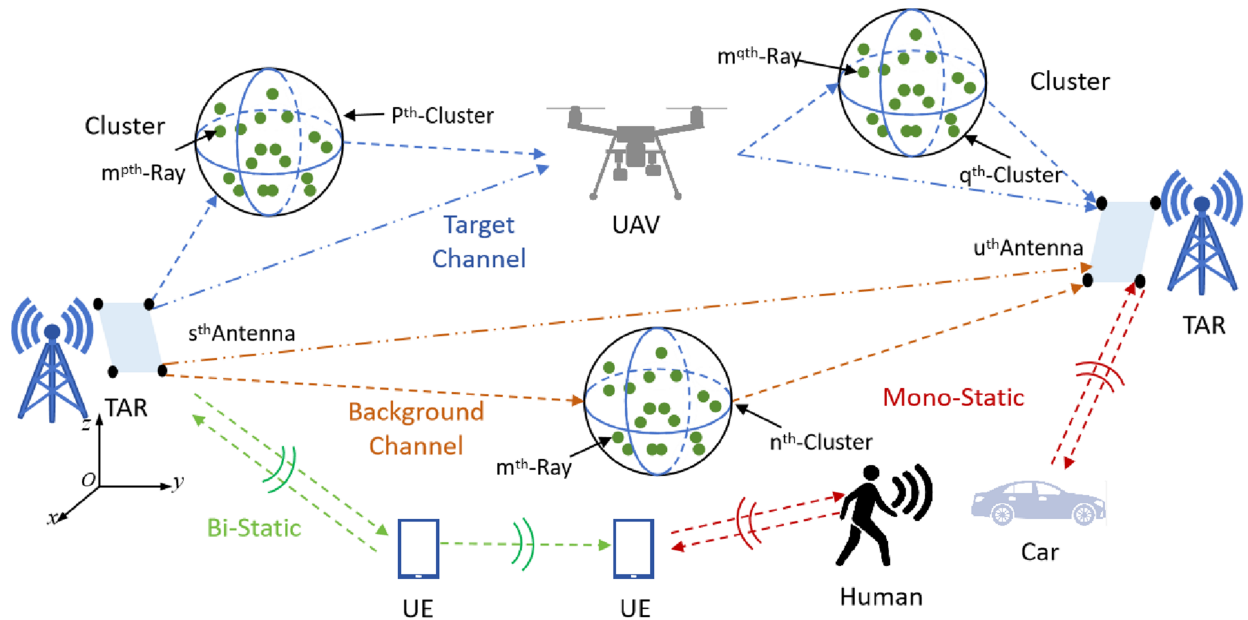


Figure 1 A geometric schematic of ISAC channel paradigm

The target channel is further classified into Tx-target and target-Rx sub-channels. In the Bi-static sensing mode, the target channel is constructed by cascading the Tx-target and target-Rx sub-channels, with parameters for each sub-channel generated according to the existing 3GPP statistical model. In the Mono-static sensing mode, the Tx-target link is generated using the 3GPP model, whereas the target-Rx components are derived by utilizing channel reciprocity. Furthermore, the background channel is generated directly using the 3GPP statistical channel model in the Bi-static sensing mode. As to the Mono-static sensing mode, the background channel can be derived from the 3GPP method, which has limited related work, or extracted through additional measurements to obtain the necessary channel model parameters.

Figure 2 depicts the proposed simulation process extended by the 3GPP channel model [13–15]. In Step 1, users are required to perform general configurations, including antenna configuration, scenario settings, target types, and the positions of the BS, UT, and targets. Steps 2 to 5 are dedicated to large-

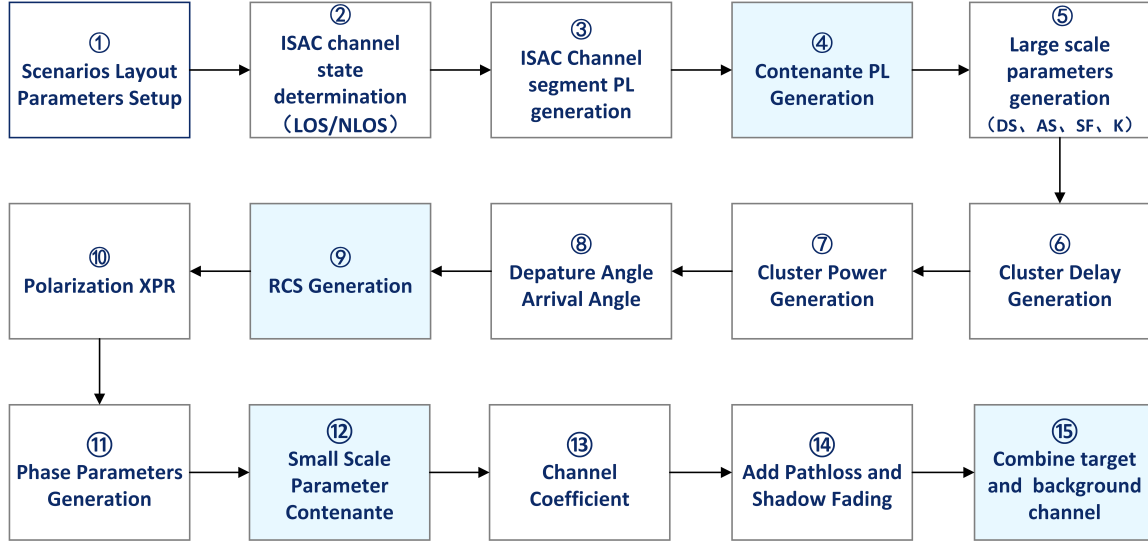


Figure 2 The simulation steps for generating ISAC channel coefficients. (changes compared to the GBSM model are highlighted)

scale parameter generation, while Steps 6 to 12 concentrate on small-scale parameter generation. Finally, Steps 13 and 14 are responsible for generating the channel coefficients. Steps 4, 9, and 12 correspond to large-scale parameter cascading, RCS generation, and small-scale parameter cascading, respectively. Step 15 refers to the combination of target and background channels.

2.1 Concatenate channel modeling

In this section, We propose a parameter cascading method for ISAC channel simulation with the scenario layouts, path loss formulas, line-of-sight (LOS) probabilities, and large-scale parameters defined in the 3GPP channel model standards TR38.901, TR36.777, and TR37.885. Specifically, TR38.901 is employed for scenarios involving human and AGV sensing targets, TR36.777 is designated for UAV target scenarios, and TR37.885 is applied to V2X target scenarios. The cascading simulation method comprises two main components: large-scale parameter cascading and small-scale parameter cascading.

2.1.1 Large scale parameters concatenate

As illustrated in Figure 2, the simulation commences with the establishment of various parameters, including the simulation scenario, target type, target position, movement speed and direction of the target, the number and location of base stations and terminals, antenna patterns, orientation angles of both base stations and terminals, system center frequency, and movement speed and direction of the terminals. For the configured scenario, the Line-of-Sight (LOS) probability and path loss for the Tx-Target and Target-Rx links are computed individually. The corresponding mean value of RCS is generated for various targets. The concatenation path loss can be calculated as

$$PL_{target}(d_1, d_2, f_0) = PL_1(d_1, f_0) + PL_2(d_2, f_0) + 10 \log \frac{c^2}{4\pi f_0^2} - 10 \log \bar{\sigma}_{RCS}, \quad (1)$$

where, d_1 and d_2 represent the distances of the Tx-target and target-Rx, respectively. f denotes the center frequency of the simulation. c is the speed of light with 3×10^8 m/s. $\bar{\sigma}_{RCS}$ is the mean RCS.

2.1.2 Small scale parameters concatenate

The total expression for channel parameters generation utilized by the BUPTCMCC-6G-CMG+ channel simulator is as

$$H_{u,s,n}(t) = \sqrt{\frac{P_n}{M}} \sum_{m=1}^M \begin{bmatrix} F_{rx,u,\theta}(\theta_{n,m,ZOA}, \phi_{n,m,AoA}) \\ F_{rx,u,\phi}(\theta_{n,m,ZOA}, \phi_{n,m,AoA}) \end{bmatrix}^T \mathbf{P} \begin{bmatrix} F_{tx,s,\theta}(\theta_{n,m,ZOD}, \phi_{n,m,AoD}) \\ F_{tx,s,\phi}(\theta_{n,m,ZOD}, \phi_{n,m,AoD}) \end{bmatrix} \exp(j \frac{2\pi}{\lambda} \hat{r}_{rx,n,m}^T \cdot \bar{d}_{rx,u}) \exp(j \frac{2\pi}{\lambda} \hat{r}_{tx,n,m}^T \cdot \bar{d}_{tx,s}) \exp(j 2\pi v_{n,m} t). \quad (2)$$

Here, P_n represents the power of the n -th cluster, generated in Step 7; M denotes the number of sub-paths within each cluster; $F_{rx,u,\theta}$ and $F_{rx,u,\phi}$ are the field components of the receiving antenna in the $\theta_{n,m,ZOA}$ and $\phi_{n,m,AOA}$ directions, respectively, while $F_{tx,s,\theta}$ and $F_{tx,s,\phi}$ are the field components of the transmitting antenna in the $\theta_{n,m,ZOD}$ and $\phi_{n,m,AOD}$ directions, respectively. \mathbf{P} is the polarization matrix. $\theta_{n,m}$ and $\phi_{n,m}$ are the vertical and horizontal angles of the m -th sub-path within the n -th cluster, generated in Step 8. $\hat{r}_{rx,n,m}$ and $\hat{r}_{tx,n,m}$ are the unit vectors in spherical coordinates, with the calculation expressions as follows

$$\hat{r}_{rx,n,m} = \begin{bmatrix} \sin \theta_{n,m,ZOA} \cos \theta_{n,m,AOA} \\ \sin \theta_{n,m,ZOA} \sin \theta_{n,m,AOA} \\ \cos \theta_{n,m,ZOA} \end{bmatrix}, \hat{r}_{tx,n,m} = \begin{bmatrix} \sin \theta_{n,m,ZOD} \cos \theta_{n,m,AOD} \\ \sin \theta_{n,m,ZOD} \sin \theta_{n,m,AOD} \\ \cos \theta_{n,m,ZOD} \end{bmatrix}, \quad (3)$$

where, $\bar{d}_{rx,u}$ and $\bar{d}_{tx,s}$ represent the position vectors of the receiving and transmitting antenna elements, respectively. $\kappa_{n,m}$ is the linear value of the cross-polarization power ratio, generated in Step 10. λ_0 is the wavelength corresponding to the carrier frequency band. and the Doppler frequency factor $v_{n,m}$ is calculated as

$$v_{n,m} = v_{n,m}^{tx-tar} + v_{n,m}^{tar-rx} = \frac{\hat{r}_{tar,n,m}^T \cdot \bar{v}_{tar} + \hat{r}_{rx,n,m}^T \cdot \bar{v}}{\lambda_0}, \quad (4)$$

where, \bar{v}_{tar} and \bar{v} represent the velocity vectors of the target and the receiver, respectively, and \mathbf{r} is the unit vector in spherical coordinates at the target's position can be expressed as

$$\hat{r}_{rx,n,m} = \begin{bmatrix} \sin \theta_{n,m,ZOA} \cos \theta_{n,m,AOA} \\ \sin \theta_{n,m,ZOA} \sin \theta_{n,m,AOA} \\ \cos \theta_{n,m,ZOA} \end{bmatrix}. \quad (5)$$

Considering that the cascaded link between the Tx-target and target-Rx involves four possible scenarios: $LOS + LOS$, $LOS + NLOS$, $NLOS + LOS$, and $NLOS + NLOS$ denoted as radio propagation case 1, 2, 3, and 4, respectively. Equation (2) presents the general channel expression under the NLOS-NLOS condition. When LOS conditions are involved, the corresponding LOS components in equation 2, such as power P_n , angles θ and ϕ , and cross-polarization power ratio, should be selectively modified according to the expressions for the LOS case in the GBSM model. Let Q and P be the number of clusters in the Tx-target and target-Rx links, respectively. The total number of clusters in the target channel is $N = QP$. For the n -th cluster of the target channel where $n = P(q-1)+p$

Cluster delay:

$$\tau_n = \tau_p + \tau_q, \quad (6)$$

where τ_p and τ_q represent the delay of the p -th and q -th cluster from Tx-target and target-Rx links respectively.

Cluster power:

$$P_n = P_p P_q, \quad (7)$$

where P_p and P_q represent the power of the p -th and q -th cluster respectively.

Doppler frequency:

$$\exp(j2\pi \frac{v_n(t)}{\lambda_0}) = \exp(j2\pi \frac{v_p(t)}{\lambda_0}) \exp(j2\pi \frac{v_q(t)}{\lambda_0}), \quad (8)$$

where $v_p(t)$ and $v_q(t)$ represent the doppler frequency of p -th and q -th links respectively.

Departure angle:

$$\theta_{n,ZoD} = \theta_{q,ZoD}, \theta_{n,AoD} = \theta_{q,AoD}. \quad (9)$$

Arrival angle:

$$\theta_{n,ZoA} = \theta_{p,ZoA}, \theta_{n,AoA} = \theta_{p,AoA}. \quad (10)$$

Polarization matrix \mathbf{P} :

$$\mathbf{P} = \begin{bmatrix} \exp(j\Phi_q^{\theta\theta}) & \sqrt{\kappa_q^{-1}} \exp(j\Phi_q^{\theta\phi}) \\ \sqrt{\kappa_q^{-1}} \exp(j\Phi_q^{\phi\theta}) & \exp(j\Phi_q^{\phi\phi}) \end{bmatrix} \mathbf{S} \begin{bmatrix} \exp(j\Phi_p^{\theta\theta}) & \sqrt{\kappa_p^{-1}} \exp(j\Phi_p^{\theta\phi}) \\ \sqrt{\kappa_p^{-1}} \exp(j\Phi_p^{\phi\theta}) & \exp(j\Phi_p^{\phi\phi}) \end{bmatrix}, \quad (11)$$

where κ_q and κ_p are the cross-polarization power ratio (XPR) in the Tx-target and target-Rx link respectively. \mathbf{S} represents the polarization matrix of the target RCS introduced in section 2.2.1.

During the 3GPP RAN 1 #116 meeting, RAN 1 defined the ISAC channel as consisting of the target and background channels. However, the methodology for generating the combined ISAC channel is subject to further study. The relationship between the background channel component and the environment channel in the absence of sensing targets remains an unresolved issue. To tackle this issue, we are introducing a new parameter called the coupling factor [23], to integrate the path loss of both the target and background channels. Consequently, the combined path loss of the ISAC channel can be expressed as follows:

$$PL_{ISAC} = PL_{target} + O_{isac} \cdot PL_{background}^{standardization}, \quad (12)$$

where the PL_{ISAC} and PL_{target} represent the linear path loss values of the ISAC channel and target channel, respectively. The $PL_{background}^{standardization}$ represents the environment channel, i.e., the initial background channel with no sensing target, and it is important to note that $PL_{background}^{standardization}$ is not the same as the defined $PL_{background}$. The latter refers to the path loss of the channel components after the target channel components have been removed. Given the similarities and compatibility with the communication channel, it is advisable to reuse the path loss model from 3GPP TR 38.901. The values of O_{isac} need further study with more measurement results.

2.2 RCS modeling

Radar systems leverage the scattered power of targets for sensing, and the accurate modeling of the RCS of these targets directly influences the performance evaluation of sensing capabilities. First, it is essential to introduce the concept of the three-dimensional resolution cell. A resolution cell is defined as the volume that is illuminated and scattered at a specific moment in time, characterized by two dimensions: angle and distance. It can be expressed as follows

$$V = \frac{\Omega R^2 c\tau}{2}, \quad (13)$$

where $\frac{c\tau}{2}$ represents the distance resolution cell, c is the speed of light, and τ is the pulse width. Ω is the antenna beam solid angle, and R is the distance from the radar receiver to the target. If the target's size is contained within the volume V , the target is considered a point target. For the five types of sensing targets defined by 3GPP UAVs, humans, long-distance vehicles, AGVs, and small road obstacles modeling as point targets is appropriate. However, for targets that exceed the resolution cell and possess irregular shapes, such as close-range vehicles and AGVs, large obstacles, and humans in gesture recognition scenarios, multi-point RCS modeling may be considered.

2.2.1 RCS polarization

The scattering characteristics of a target are influenced by the polarization of the incident field. When the antenna is linearly polarized, the incident linearly polarized wave on the target surface can be decomposed into vertical and horizontal polarization components. The polarization components of the scattered field from the target, as received by the receiving antenna, can be expressed as

$$\begin{bmatrix} E_H^R \\ E_V^R \end{bmatrix} = \begin{bmatrix} \alpha_{HH} & \alpha_{VH} \\ \alpha_{HV} & \alpha_{VV} \end{bmatrix} \begin{bmatrix} E_H^T \\ E_V^T \end{bmatrix}, \quad (14)$$

where E_H^R and E_V^R denote the horizontally and vertically polarized components of the received electric field, respectively, E_H^T and E_V^T denote the horizontally and vertically polarized components of the transmitted electric field, respectively. The scattering matrix \mathbf{S} represents the coefficients related to the target's scattering characteristics and polarization.

2.2.2 RCS modeling based Measurement

Drawing upon the comprehensive analysis of measurements that depend on frequency, distance, and target type conducted by our team in [24, 25], the following conclusions regarding RCS modeling can be established:

- The RCS of the UAV is independent of angle and demonstrates characteristics akin to omnidirectional scattering. Furthermore, the measurement results obtained from both Mono-static and Bi-static modes closely approximate each other.

- The RCS model for the UAV is represented as a normal distribution in both Mono-static and Bi-static sensing modes. The mean defines the deterministic component, while the variance characterizes the stochastic component.

- The RCS of a human is angle-independent and displays characteristics akin to omnidirectional scattering. Furthermore, the measurement results obtained from Mono-static and Bi-static modes closely align with each other.

- The RCS model for humans is represented as a normal distribution in both Mono-static and Bi-static sensing modes. The mean value characterizes the deterministic component, while the variance accounts for the stochastic component.

For different types of sensing targets, our team has proposed a unified RCS modeling framework in RAN1 #118bis meeting [26]:

$$RCS = A \times B_1 \times B_2, \quad (15)$$

where A component is included in the large scale and is a deterministic value. The B_1 component is included in the small scale and is a deterministic angle-dependent value or scattering pattern based on measurements. The B_2 component is a normal distribution with a mean and variance. Modeling the RCS of a UAV based on this framework, since its RCS is angle-dependent, the A component is set to the mean or peak value, or simply set to 1, etc., the B_1 component is a function related to the angle, and B_2 is a random value independent of the angle, representing the fluctuation of RCS. This model framework can effectively model the RCS of sensing targets with different scattering patterns, so we simulate with subsequent discussions on RCS modeling for different sensing targets based on this model framework.

Different from the human body and small UAV, vehicle RCS and large UAV exhibit spiking characteristics that render them unsuitable for modeling with omnidirectional patterns. The RCS of humans and small UAVs can be modeled using A and B_1 with a log-normal distribution, in which the mean μ and variance σ are determined from empirical measurements. The RCS of vehicles and large UAVs displays four distinct peaks in its angular distribution, highlighting the need for further investigation into B_1 and simulation methodologies. The conversion formula for single-station and dual-station RCS values is as follows:

$$RCS_{Bi} = RCS_{Mono} \cos \frac{\beta}{2}. \quad (16)$$

This equation is valid under the condition that the target is sufficiently smooth and free from shadowing and back-scatter effects. It necessitates validation through measurement results and can be modeled analogous to an antenna radiation pattern.

3 Metrics for ISAC Evaluation

3.1 Accuracy metric

Table 2 Basic metrics for sensing

Sensing usage	Principle	Accuracy	Resolution
Ranging	$R = \frac{1}{2}ct_R$	$dR = \frac{1}{2}cdt_R + \frac{R}{C}dc$	$\Delta R = \frac{1}{2}ct_\tau$
Speed detection	$f_d = \frac{2v}{\lambda}$	$dv = \frac{\lambda}{2}df_d$	$\Delta v = \frac{\lambda}{2}\Delta f_d$
Angulation	$d\theta = \arcsin(\frac{\phi\lambda}{2\pi d})$	$d\theta = \frac{\lambda d\phi}{2\pi d \cos \theta}$	$\Delta\theta > \frac{\lambda}{Nd \cos \theta}$

The fundamental detection equation in radar is presented in Table 2. Here, c is the speed of light and t_R represents the time interval between the transmitted pulse and the received echo pulse from the sensed target. The ranging accuracy can be qualitatively analyzed using the total differential expression as defined in Table 2. The range resolution ΔR is defined as the minimum distinguishable distance, which is related to the pulse width t_τ of the sensing signal. The maximum unambiguous range is determined by the pulse repetition interval T_R and is expressed as follows:

$$R_{Max} = \frac{1}{2}cT_R, \quad (17)$$

$$R = \frac{1}{2}c(mT_R + t_r). \quad (18)$$

The basic principle of angle measurement in the radar field is as follows

$$\phi = \frac{2\pi}{\lambda}d \sin \theta, \quad (19)$$

where ϕ represents the phase difference between different antenna elements that are separated by a distance d at the receiver and θ is the angle of the sensing target. The angle measurement accuracy can be expressed as

$$d\phi = \frac{2\pi}{\lambda}d \cos \theta d\theta, \quad (20)$$

$$\phi = \frac{2\pi}{\lambda}d \sin \theta < \pi. \quad (21)$$

Based on equation (21), we can drive $\theta_{max} = \arcsin(\frac{\lambda}{2\pi})$. The angle resolution $\Delta\theta$ is defined as the minimum distinguishable angle, which is related to the main lobe width of the antenna array $\frac{2\pi}{N}$. The basic principle of velocity measurement is based on the Doppler frequency. From Table 2, we obtain $v = \frac{\lambda f_d}{2}$. Analogous to range resolution and angular resolution, Doppler resolution can be expressed as $\Delta f_d = \frac{1}{MT_R}$, in which M is the number of transmitted pulses, and T_R is the pulse repetition interval.

3.2 Detection metric

The probability of false alarms arises when the noise at the receiver surpasses the decision threshold, resulting in erroneous detection. This probability is associated with the root mean square (RMS) value of the noise and the decision threshold, and it is defined as follows

$$P_{fa} = \int_{V_T}^{\infty} \omega(x|\text{no target})dx, \quad (22)$$

where V_T is the decision threshold, $\omega(x)$ denotes the probability density function (PDF) of detection. When the noise is complex and both its real and imaginary components follow a Gaussian distribution, the magnitude of the noise follows a Rayleigh distribution, $\omega(x)$ can be expressed as

$$\omega(x|\text{no target}) = \frac{x}{\sigma^2} \exp(-\frac{x^2}{2\sigma^2}), x \geq 0. \quad (23)$$

Substituting equation (23) into equation (22) results in

$$P_{fa} = \exp(-\frac{V_T^2}{2\sigma^2}). \quad (24)$$

Further, the relationship between P_{fa} and V_T is obtained as $V_T = \sqrt{2\sigma^2 \ln P_{fa}}$. The probability of detection, P_D , represents the likelihood of correctly detecting a target when one is present and is defined as follows

$$P_D = \int_{V_T}^{\infty} \omega(x|\text{has target})dx = \int_{V_T}^{\infty} \frac{x}{\sigma} \exp(-\frac{A^2 + x^2}{2\sigma^2}) J_0(\frac{AX}{\sigma^2}) dx. \quad (25)$$

4 Simulation Results

In the simulation experiments, the primary focus is on the reliability of the ISAC channel cascading method and the accuracy of the RCS simulation results. RAN1 118 bis meeting has agreed 8 options for concatenating the Tx-target and target-Rx link in the target channel as

- Direct path (if present) is always kept
- Indirect paths of LOS+NLOS, NLOS+LOS (if present) are generated
- On other indirect paths of NLOS + NLOS
- Option 0: ray level full convolution between Tx-target and target-Rx link for Case 1/2/3/4.
- Option 0A: ray level full convolution between Tx-target and target-Rx link only for Case 4.

- Option 1: cluster level full convolution between Tx-target link and target-Rx link, then 1-by-1 coupling rays within each pair of clusters for Case 1/2/3/4.
- Option 1A: cluster level full convolution between Tx-target and target-Rx link, then 1-by-1 coupling rays within each pair of clusters only for Case 4.
- Option 2: cluster level 1-by-1 coupling between Tx-target and target-Rx link, then 1-by-1 coupling rays within each pair of clusters for Case 1/2/3/4.
- Option 2A: cluster level 1-by-1 coupling between Tx-target and target-Rx link, then 1-by-1 coupling rays within each pair of clusters only for Case 4.
- Option 2A: ray level 1-by-1 coupling between Tx-target and target-Rx link for Case 1/2/3/4.
- Option 3A: ray level 1-by-1 coupling between Tx-target and target-Rx link only for Case 4.

Metrics defined for the target channel include power, delay spread (DS), and angle spread (ASA, ASD, ZSA, ZSD). Based on the concatenation methods at the cluster level, ray level, random coupling, and order coupling, the 8 options above can be further subdivided into 10 cases: Options 0, 1, 2, and 3A in

Table 3 Simulation cases for concatenation

CaseA	Concatenation only for radio propagation NLOS-NLOS
Case0	Full convolution between Tx-target link and target-Rx link
Case1	Cluster full convolution, then 1-by-1 coupling rays within each pair of clusters
Case2O	Cluster level 1-by-1 coupling, then 1-by-1 coupling rays in order within each pair of clusters
Case2R	Cluster level 1-by-1 coupling, then 1-by-1 randomly coupling rays within each pair of clusters
Case3	Ray level 1-by-1 randomly coupling between Tx-target link and target-Rx link
Case1N	Cluster full convolution, 1-by-1 coupling rays (NLOS-NLOS normalization)
Case2ON	Cluster level 1-by-1 coupling, 1-by-1 coupling rays in order (NLOS-NLOS normalization)
Case2RN	Cluster level 1-by-1 coupling, then 1-by-1 randomly coupling rays (NLOS-NLOS normalization)
Case3N	Ray level 1-by-1 randomly coupling between Tx-target link and target-Rx link (NLOS-NLOS normalization)

#118-bis simulation options for concatenation are uniformly represented by CaseA. The ray-level 1-by-1 coupling in order is excluded, as it is equivalent to Case 2O. Additionally, the specific coupling method of ray 1-by-1, whether sequential or random, does not affect Case 1, Case 2O, or Case 2R. This is because the power of each ray pair depends solely on the power of the corresponding clusters, with rays within the same cluster having equal power. Therefore, the coupling method at the ray level does not affect the distribution, as the power of each ray pair remains the same once the cluster-level concatenation is complete. The simulation configuration parameters and corresponding results are presented as Table 4.

In the simulation, we assume that the total coupling number is determined by selecting the minimum number of clusters when the Tx-target and target-Rx links have differing numbers of clusters (e.g., 12 clusters for UMi-LOS and 19 clusters for UMi-NLOS, selecting the smaller value of 12). As observed in Figure 3, Case 1, Case 2O, and Case 2R exhibit a lower power percentage compared to Case 0 (Full Convolution), and overall normalization does not affect the statistical distribution of the spread values (DS and AS). The performance of random coupling at the cluster level (Case 2R) is closer to that of Case 0 than the performance of ordered coupling (Case 2O). As observed in LOS case2 and LOS case3 (LOS+NLOS and NLOS+LOS conditions), reserving only the paths associated with LOS paths in Case A results in a zero value for angle spread in the link where the LOS path resides either the Tx-target link or the target-Rx link. Importantly, we observe that the results approximate Case 0 as Case 1N, 2ON, and 2RN by normalizing the power of NLOS-NLOS in Case 1, 2O, and 2R. Furthermore, Case 1N (full convolution at the cluster level followed by normalization) and Case 0 (full convolution) are identical. The CDF curves of case 1N, 2ON, 2RN, and 3N are similar in LOS case 1 (LOS-LOS condition). Case1N exhibits statistical characteristics identical to Case0 (full convolution), while Case2RN closely approximates the distribution of full convolution than Case2ON. In conclusion, As for the concatenation of the target channel, normalization of the NLOS-NLOS paths is necessary to maintain the parameter distribution of the channel across different simulation options. Meanwhile, the performance of random coupling in simulation option 2 (Cluster 1-by-1 randomly coupling) is superior to sequential coupling, so random coupling can be prioritized.

Figure 4 illustrates the human target's RCS simulation and measurement results at 5 GHz, 14 GHz, and 28 GHz in Mono-static mode. The simulated results demonstrate a good alignment with the measured

Table 4 Simulation setups

Scenarios	UMi in 3GPP TR38.901
Sensing mode	Bi-static
Frequency	6GHz
RCS model	$RCS = A * B_1 * B_2 = 1$

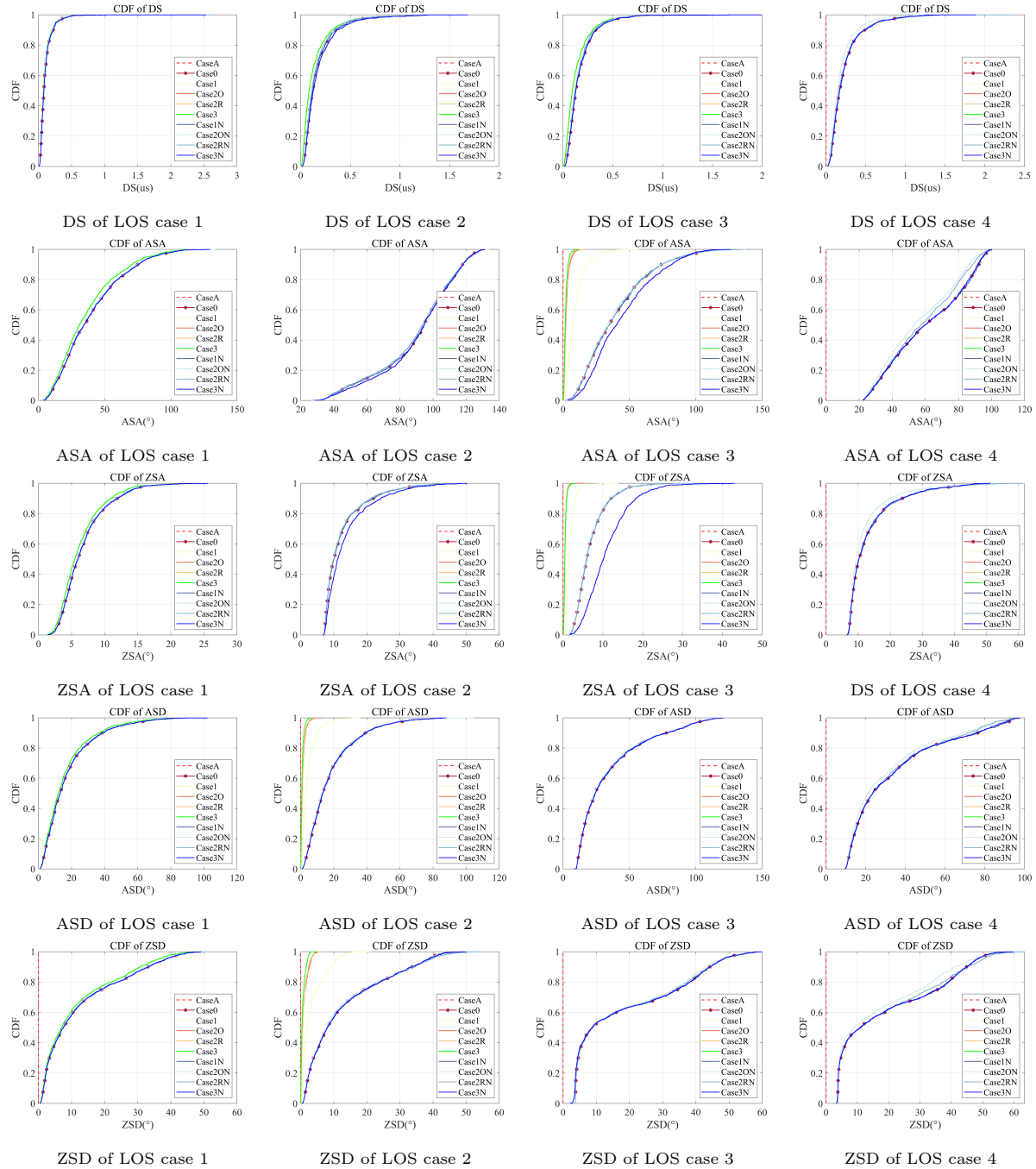


Figure 3 Simulation results for concatenation in UMi scenario

results reported in reference [25], thereby validating the feasibility of the log-normal fitting scheme. Additionally, this finding confirms the differences in RCS distribution between ISAC channels and traditional radar systems. This discrepancy arises from the fact that traditional radar RCS perception typically occurs at greater distances, while ISAC services are concentrated on closer ranges. Consequently, it results

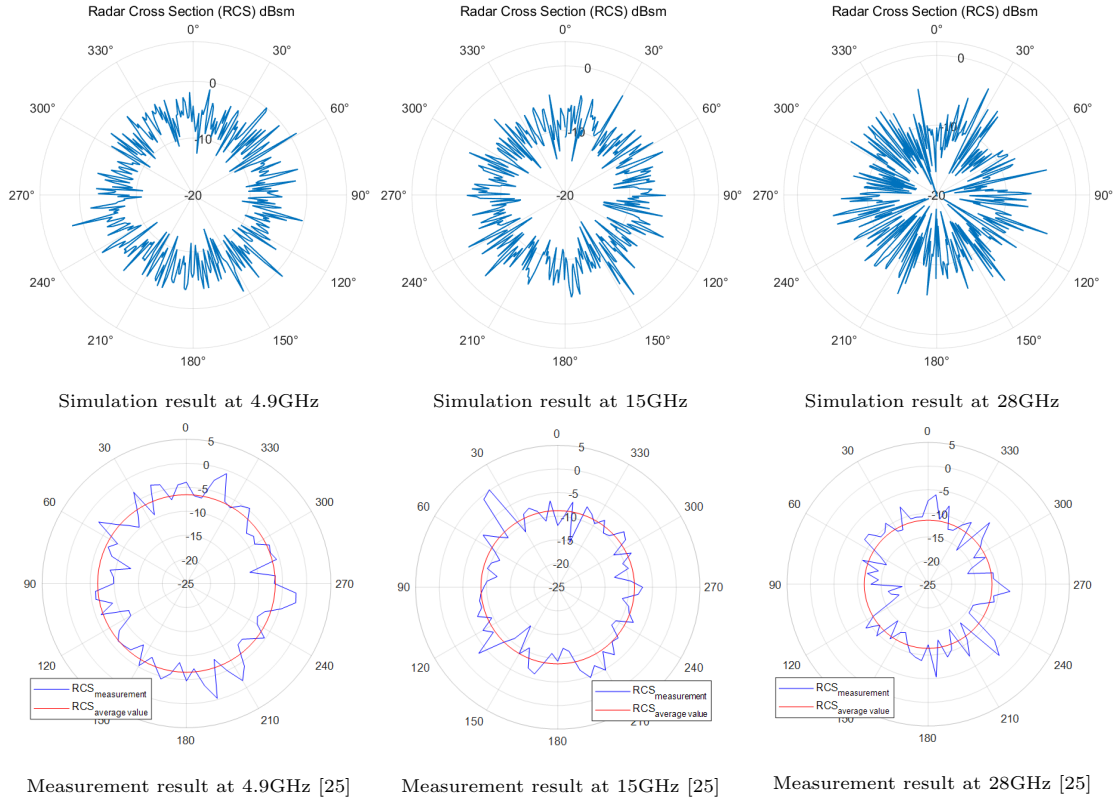


Figure 4 RCS measurements and simulation results of human target at 4.9GHz, 15GHz, and 28 GHz in Mono-static mode.

in variations between the RCS distributions observed in radar applications and those measured in ISAC.

5 Conclusion

In this paper, we extend the 3GPP GBSM standard channel model by incorporating the latest advancements in 3GPP ISAC standardization, thereby enhancing the integrated sensing and communication channel simulation capabilities for 6G. The new model accommodates both Bi-static and Mono-static sensing modes, supporting four types of sensing targets: UAVs, vehicles, humans, and AGVs. This model aligns with prime options outlined in the 3GPP standardization progress, including methods for modeling RCS size and scale, polarization, and a combination of target and background channels.

Through down-selection simulations of the 8 concatenation options provided in the #118-bis meeting, we observed the relation between different cascading methods compared to the fully convoluted baseline. NLOS-NLOS power normalization should be performed, as it ensures overall small-scale power normalization and brings the statistical characteristics of different cascading options closer to option 0. After NLOS-NLOS power normalization, the statistical distribution of option 1 matches exactly with that of option 0. In option 2, the random matching method performs better than the sequential coupling method. Option 3 fits the fully convoluted result better than option 2. However, option 3 abandons the traditional cluster concept. If the cluster concept is necessary (e.g., for MIMO OTA testing), we recommend using option 2, which retains the cluster concept while closely approximating the fully convoluted results.

This advancement accelerates the standardization of the 6G ISAC channel model and the evaluation of novel algorithms, as it enables the utilization of existing 5G standard parameter tables alongside the proposed cascading model and measured RCS data to simulate ISAC channels. The unified simulation framework applies to all future developments in ISAC channel model standardization, offering insights into the standardization simulation process and facilitating the progress of simulation evaluations.

Future research is required to investigate background channel modeling in the Mono-static sensing mode, as well as the spatial consistency modeling in the ISAC channel. Furthermore, calibration and RCS parameters should be revised following the latest developments in standardization.

Acknowledgements This work was supported in part by the National Natural Science Foundation of China (Grant Nos. 61925102, 62201087, and 62341128), in part by the National Key R&D Program of China (Grant No. 2023YFB2904805), in part by the Beijing Natural Science Foundation - Xiaomi Innovation Joint Fund (Grant No. L243002) and in part by Guangdong Major Project of Basic and Applied Basic Research (Grant No. 2023B0303000001).

References

- 1 ITU, "Future technology trends of terrestrial International Mobile Telecommunications systems towards 2030 and beyond," ITU-R M.2516, Nov. 2022.
- 2 ITU, "IMT Vision-Framework and overall objectives of the future development of IMT for 2030 and beyond," ITU-R M.[IMT.VISION 2030 AND BEYOND].
- 3 Li H, Xu J, Sun C, et al. Integrated sensing and communication: 3GPP standardization progress[C]//2023 21st International Symposium on Modeling and Optimization in Mobile, Ad Hoc, and Wireless Networks (WiOpt). IEEE, 2023: 1-7.
- 4 Liu, G., Xi, R., Han, Z., et al.: Cooperative Sensing for 6G Mobile Cellular Networks: Feasibility, Performance and Field Trial. *IEEE J.Sel. Areas Commun.*, Early Access (2024).
- 5 Zhang, J., Wang, H., Zhang, Y., et al.: Channel characteristics and modeling research for 6G: challenges, progress, and prospects (in Chinese). *Sci Sin Inform.*, 2024, 54(5):pp. 1114-1143
- 6 J. Wang, N. Varshney, C. Gentile, S. Blandino, J. Chuang, and N. Golmie, "Integrated Sensing and Communication: Enabling Techniques, Applications, Tools and Data Sets, Standardization, and Future Directions," *IEEE Internet of Things Journal*, 2022, vol. 9:23416– 23440.
- 7 Wang H, Zhang J, Nie G, et al. Digital Twin Channel for 6G: Concepts, Architectures and Potential Applications[J]. arXiv preprint arXiv:2403.12467, 2024.
- 8 Yang H, Feng Z, Wei Z, et al. Intelligent computation offloading for joint communication and sensing-based vehicular networks[J]. *IEEE Transactions on Wireless Communications*, 2023.
- 9 F. Liu, Y. Cui, C. Masouros, J. Xu, T. X. Han, Y. C. Eldar, and S. Buzzi, "Integrated Sensing and Communications: Toward Dual Functional Wireless Networks for 6G and Beyond," *IEEE Journal on Selected Areas in Communications*, 2022, vol.40:1728–1767.
- 10 J. Zhang, P. Tang, L. Yu, T. Jiang, and L. Tian, Channel measurements and models for 6G: current status and future outlook, *Frontiers of Information Technology & Electronic Engineering*, 2020, vol. 21: 39–61.
- 11 J. Zhang, Y. Zhang, Y. Yu, R. Xu, Q. Zheng, and P. Zhang, "3-D MIMO: How Much Does It Meet Our Expectations Observed From Channel Measurements?," *IEEE Journal on Selected Areas in Communications*, 2017, vol. 35:1887–1903.
- 12 Zhang J, Lin J, Tang P, et al. Channel measurement, modeling, and simulation for 6G: A survey and tutorial[J]. arXiv preprint arXiv:2305.16616, 2023.
- 13 3GPP, "Study on channel model for frequencies from 0.5 to 100 GHz (Release 15)," tech. rep., 3GPP TR 38.901, 2018.
- 14 3GPP, "Study on Enhanced LTE Support for Aerial Vehicles(Release 15)," tech. rep., 3GPP TR 36.777, 2017.
- 15 3GPP, "Study on evaluation methodology of new Vehicle-to- Everything (V2X) use cases for LTE and NR(Release 15),"tech. rep., 3GPP TR 37.885, 2019.
- 16 ITU, "Guidelines for evaluation of radio interface technologies for IMT-2020," ITU-R M.2412, Oct. 2017.
- 17 3GPP TSG SA: Feasibility Study on Integrated Sensing and Communication. 3GPP TR 22.837 (2024). Available from: <https://portal.3gpp.org/desktopmodules/Specifications/SpecificationDetails.aspx?specificationId=4044>.
- 18 Zhang Z, He R, Ai B, et al. A general channel model for integrated sensing and communication scenarios[J]. *IEEE Communications Magazine*, 2022, 61(5): 68-74.
- 19 Liu Y, Zhang J, Zhang Y, et al. A Shared Cluster-based Stochastic Channel Model for Integrated Sensing and Communication Systems[J]. *IEEE Transactions on Vehicular Technology*, 2023.
- 20 Xiong B, Zhang Z, Ge Y, et al. Channel modeling for heterogeneous vehicular ISAC system with shared clusters[C]//2023 IEEE 98th Vehicular Technology Conference (VTC2023-Fall). IEEE, 2023: 1-6.
- 21 Han J, He D, Pan R, et al. Terahertz channel modeling for integrated sensing and communication[C]//2023 IEEE 24th International Workshop on Signal Processing Advances in Wireless Communications (SPAWC). IEEE, 2023: 651-655.
- 22 Li X, He J, Yu Z, et al. Rough-surface scattering theory and modeling for 6G ISAC[C]//2022 IEEE Globecom Workshops (GC Wkshps). IEEE, 2022: 1310-1316.
- 23 W.Chen, Y.Zhang, Y.Liu, J.Zhang, H.Gong, T.Jiang, L.Xia, "An empirical study of ISAC channel characteristics with human target impact at 105 GHz," *Electronic Letter*, 2024, vol.60: e70017.
- 24 BUPT, CMCC, R1-2404417, Discussion on ISAC channel modeling, 3GPP TSG RAN WG1 #117, May 20th – May 24th, 2024.
- 25 BUPT, CMCC,VIVO, R1-2406107, ISAC Channel Measurements and Modeling,3GPP TSG RAN WG1 #118, Aug 19th – Aug 23th, 2024.
- 26 BUPT, CMCC, R1-2408263, ISAC Channel Modeling and Measurement Validation,3GPP TSG RAN WG1 #118-bis, Oct 14th – Oct 18th, 2024.